Calibration of the Airborne Visible/Infrared Imaging Spectrometer in the Laboratory

Thomas G. Chrien, Robert O. Green, Christopher J. Chovit,
Michael L. Eastwood, and Charles M. Sarture

Jet Propulsion Laboratory, California Institute of Technology, Pasadena, CA 91101

1.0 Introduction

Imaging spectrometry data must be spectrally, radiometrically and geometrically calibrated in order to: 1) derive physical parameters from measured spectral radiance, 2) compare data acquired from different regions and from different times, 3) compare and analyze the imaging spectrometry data with data acquired from other calibrated sensors, and 4) compare and analyze data with results from computer models. The calibration of AVIRIS data is the process by which laboratory characterization data is applied to raw instrument data (digitized number versus spectral channels) to produce instrument independent, quantitative spectra (radiance versus wavelength) for each image pixel. "The AVIRIS sensor and calibration process is described by Vane (Vane et al., 1993) and the application of the calibration data to the raw digital data is described by Green (Green et al., 1992).This calibration process is validated for in-flight performance of the sensor using a rigorous ground truth campaign (Green, 1996).

This workshop paper reviews the laboratory characterization data set which is used in the AVIRIS calibration process. The laboratory measurements used to acquire the calibration data are divided into three classes: 1) spectral calibration, 2) radiometric calibration, and 3) spatial calibration.

2.0 Spectral Calibration

The collection of spectral calibration data for AVIRIS was first described by Vane (Vane et al., 1987) and then updated by Chrien (Chrien et al., 1990). Green updated the spectral calibration requirement of AVIRIS to 0.1 nm in center wavelength and FWHM knowledge (Green, 1995) based on a sensitivity to the ubiquitous narrow solar and atmospheric absorption in the upwelling spectral radiance. The method is to measure the response of each of the 224 AVIRIS channels to narrow bandwidth light (1-2 nm FWHM) as it is scanned in wavelength across the approximately -t/- 15 nm about the center wavelength. This is accomplished by using a monochromator and collimator as shown in Figure 1. (a). A four parameter Gaussian function is fit to each channel spectral response from which the center wavelength and FWHM channel width is derived. An automated process is used to collect the spectral response data for all 224 spectral channels and to calibrate the monochromator prior to and afterwards. The monochromator calibration is traced to Mercury vapor, Neon and Krypton emission lamps.

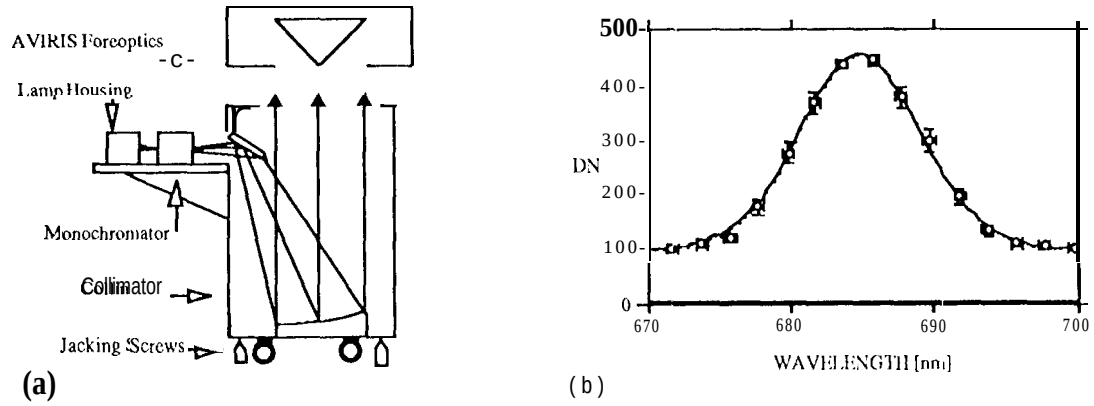

FIGURE 1. a) Laboratory spectral calibration Set-llp, b) Typical spectral response function with error bars and best fit Gaussian curve from which center wavelength, FWHM bandwidth and uncertainties are derived.

The center wavelength for each of the 224 spectra] channels shown in Figure 2. (bold line) where discontinuity in the line denotes the spectral overlap between the four AVIRIS spectrometers. The associated uncertainty in the determination of center wavelength is shown on the same plot by reading the right axis. A majority of the channels meet the calibration goal of uncertainty less than 0.1 nm in absolute knowledge of center wavelength.

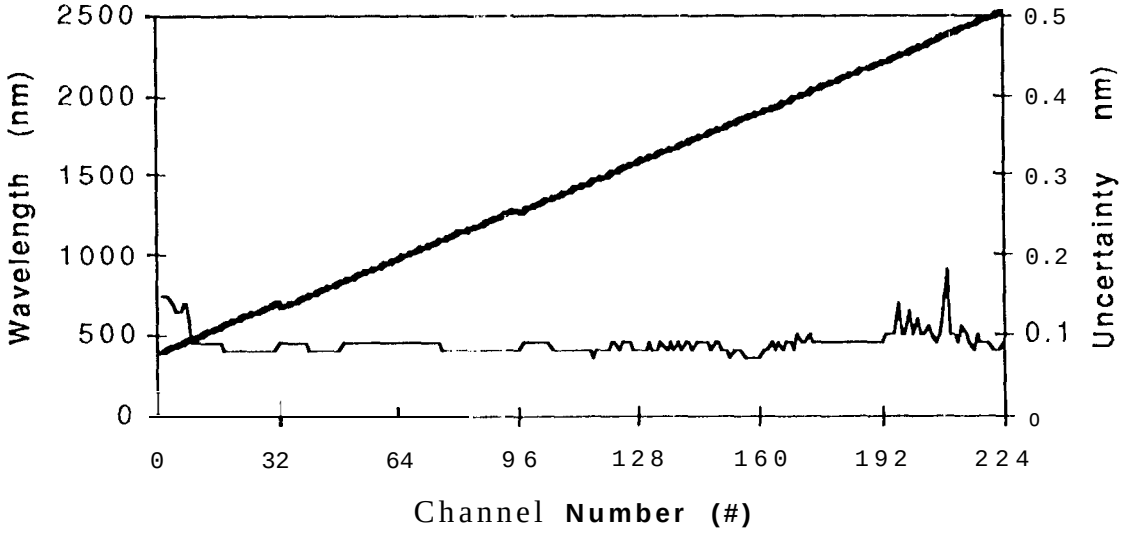

FIGURE 2. Derived center wavelengths for each AVIRIS channel (bold line), read from left axis, and associated uncertainty in center wavelength knowledge (normal line), read from right axis.

The best-fit Gaussian FWHM bandwidth for each of the 224 spectral channels is shown in Figure 3. (bold line) The associated uncertainty in the determination of FWHM bandwidth is shown on the same plot by reading the right axis. A majority of the channels meet the calibration goal of uncertainty less than 0.1 nm in knowledge of bandwidth.

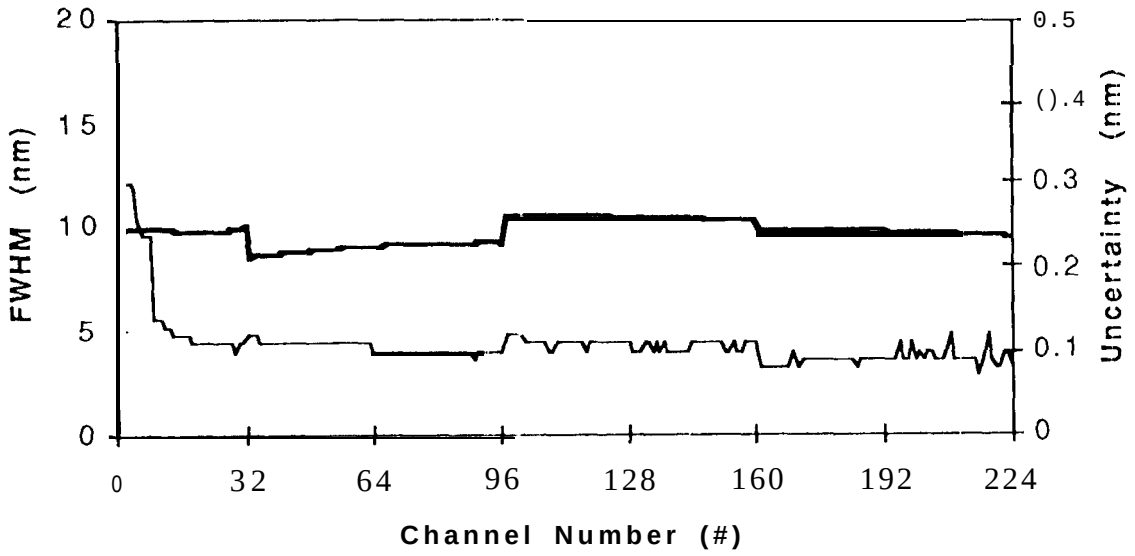

FIGURE 3. Derived FWHM bandwidth for each AVIRIS channel (bold line), read from left axis, and associated bandwidth uncertainty (normal line), read from right axis.

The in-flight calibration of the spectral response has been validated using a least-squares curve fit to atmospheric features over a carefully characterized field targets such as Lunar Lake, Nevada, and Rogers Dry Lake, California (Green, 1995; Green et al., 1993). The AVIRIS onboard Calibration system can also be used to monitor minute changes in the spectral response by computing the transmittance of the spectrally feature-full filters and observing shifts with respect to filter data acquired at the time of the laboratory calibration (Chrien, 1995).

3.0 Radiometric Calibration

The absolute radiometric calibration of the AVIRIS sensor is determined by measuring the radiometric response of the sensor to a standard of known spectral radiance. The standard is constructed from a NIST-traceable irradiance standard lamp and a NIST-traceable reflectance standard panel as shown in Figure 4. The spectral radiance of the standard is computed using Equation 1.:

$$L(\lambda) = \frac{E(\lambda) R(\lambda)}{\pi} \qquad \text{(EQ 1)}$$

$L(\lambda)$ is the target radiance as viewed by the spectrometer and $E(\lambda)$ is the lamp irradiance at a distance of 50 cm from a panel with reflectance $R(\lambda)$. The spectral radiance of the standard is shown in Figure 5. along with the associated percent uncertain as computed using error propagation in Equation 1. "The AVIRIS sensor views the standard directly and the mean of over 1000 digital number (dn) per channel measurements of the standard is computed. "The mean and percent uncertainty of this measurement is shown in Figure 6. The

high signal-to-noise ratio of the AVIRIS sensor combined with the laboratory luxury of averaging results in extremely low percent uncertainty across most wavelengths.

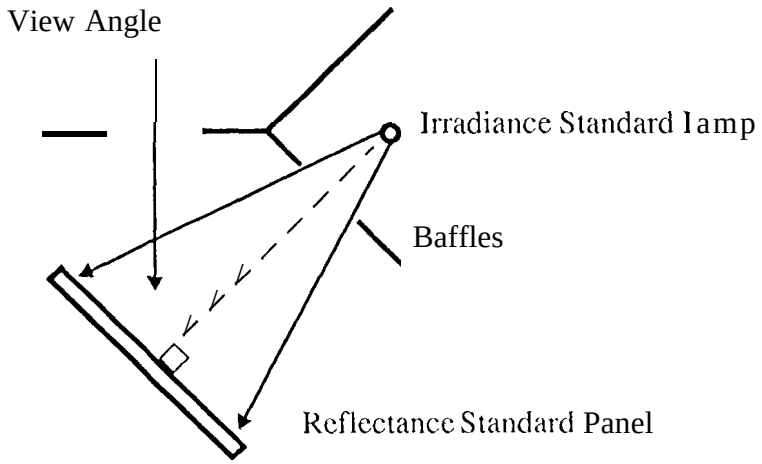

Viewing geometry for NISrl'-traceablc radiancestandard.

Radiometric calibration coefficients are computed by dividing the standard radiance by the sensor dn response. The results arc shown in Figure 7. along with the root-sum-square (RSS) uncertainty of standard radiance and sensor response. The RSS uncertainty is dominated by the radiance standard uncertainty except at wavelengths below 430 nm where the sensor response uncertainty becomes significant. These radiometric gain coefficients are applied to inflight image data to produce calibrated image radiance. An additional onboard calibrator correction factor may be applied to compensate for minor drifts in spectrometer response (Green, 1993).

"l'he radiometric gain coefficients are validated in-flight using a series of calibration experiments typically scheduled for the start, middle and end of the flight season (Green et al., 1996; *Green* et al., 1993). The field experiment is used to predict the upwelling radiance at the AVIRIS sensor via an independent calibration path which relics on measurements of playa reflectance, atmospheric optical depth, and the MODTRAN3 radiative transfer code (Anderson. 1995). 1 'igure 8. compares the measurement uncertain y (bold line) derived as the RSS of calibration uncertainty (normal line) and the percent variation in the measured spectrum due to instrument noise, atmospheric, and playa variability to the percentage difference between the laboratory calibrated spectra and the Modtran3 constrained independent prediction of radiance. The actual difference to the prediction is strongly influenced by many factors including errors in the MODTRAN3 line list and algorithm, minute errors in the AVIRIS spectral calibration, and instabilities in the field spectrometer used in the playa reflectance measurements. The point to note is that in spite of the many unknowns in the MODTRAN3 prediction, the level of agreement is better than the error analysis derived uncertainty in many parts of the spectrum. This suggests that the NIST calibration uncertainty is overstated, especially in the 2100 to 2450 nm spectral region

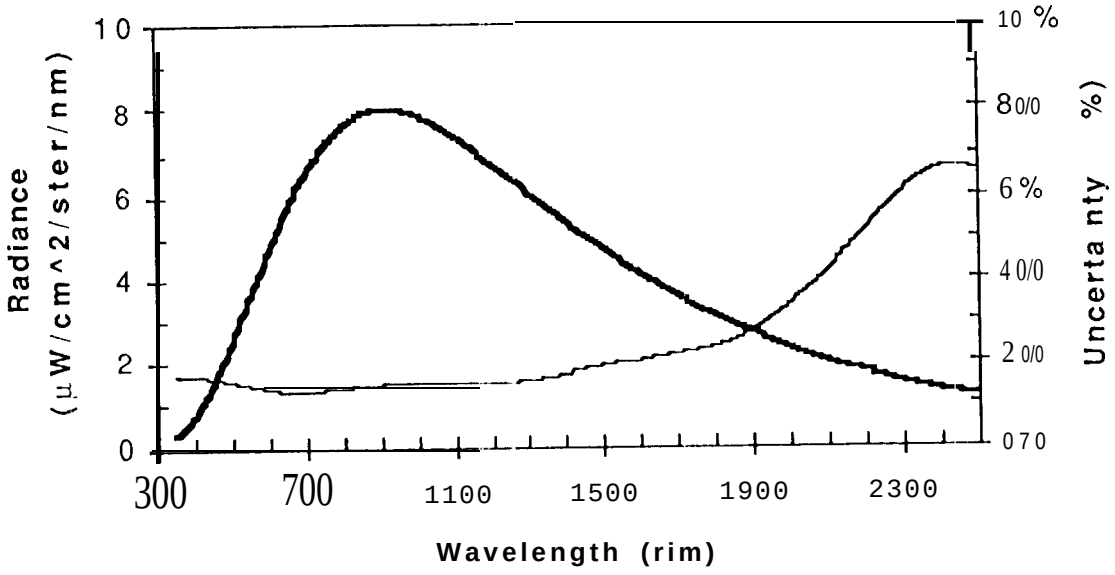

FIGURE 4. NIST traceable radiance standard target radiance (bold line), read from left axis, and percent radiometric uncertainty (normal line), read from right axis.

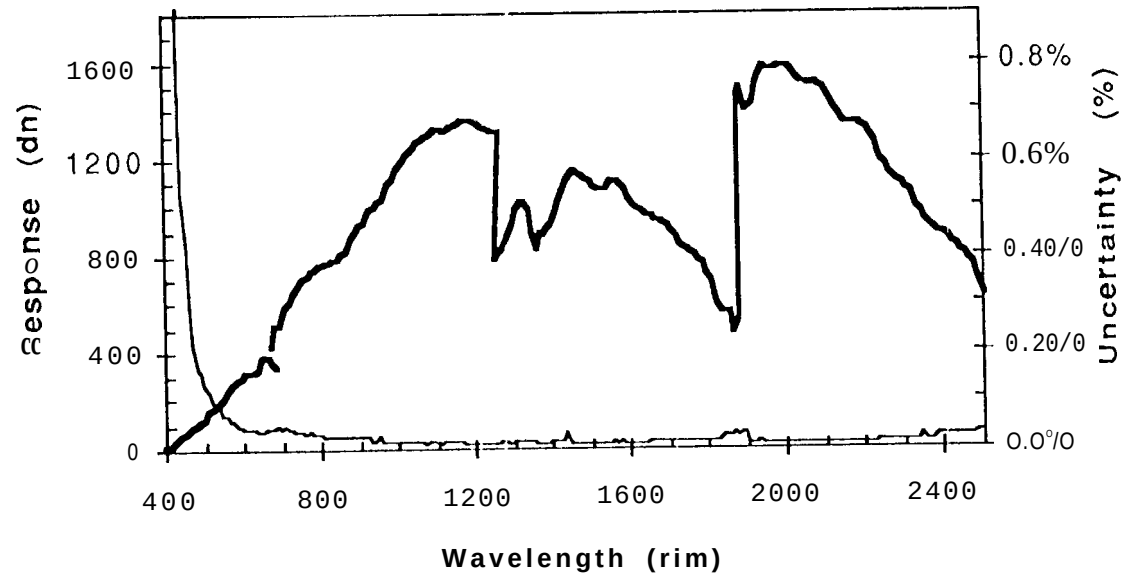

FIGURE S. AVIRIS digital number (dn) response to NISrl'-traccable radiance standard (bold line), read from left axis, and percent uncertainty of response doe to measurement noise (normal line), read from right axis.

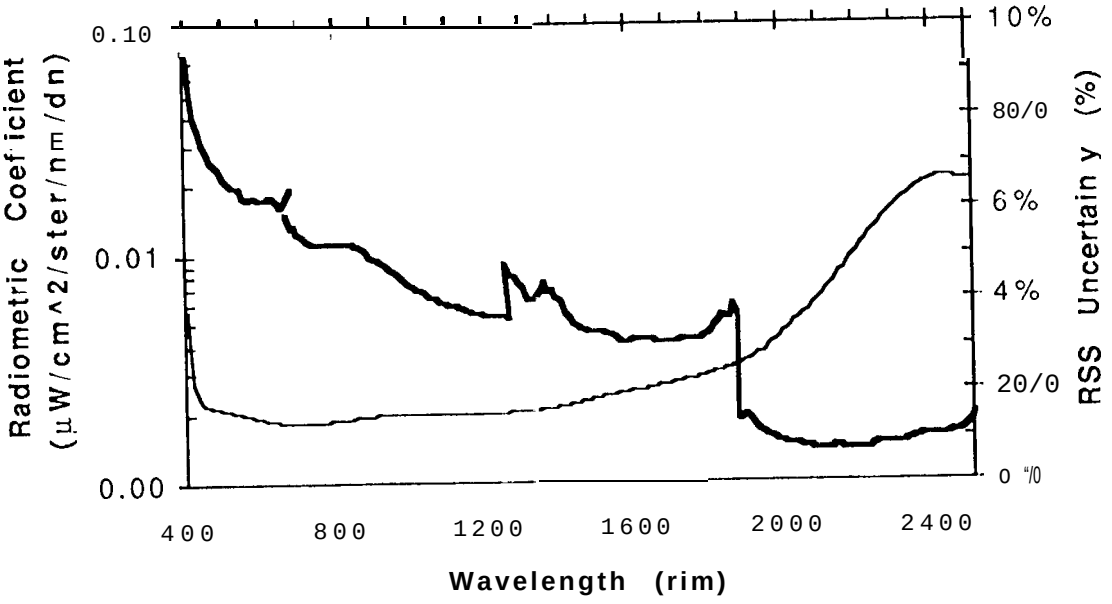

FIGURE 6. Radiometric calibration coefficients derived by dividing the NIST-traceable standard radiance by the AVIRIS radiometric square (RSS) percent uncertainty (normal line), read from right axis, and root sum standard (bold line), read from left axis,

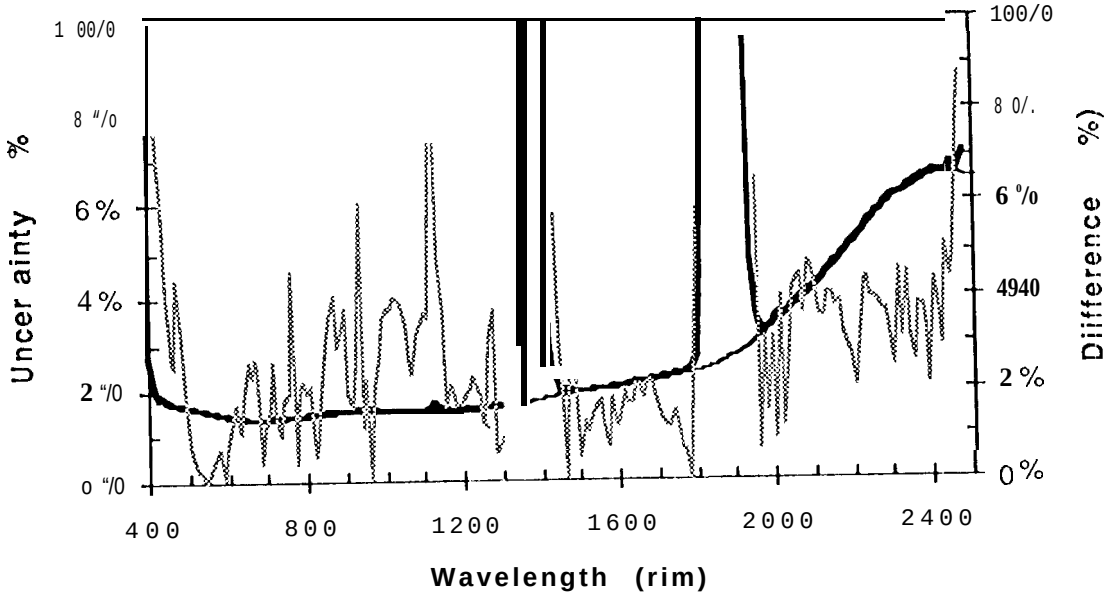

FIGURE 7. Measurement uncertainty (bold line) derived as the RSS of calibration uncertainty (normal line) and the percent variation in the measured spectrum due to instrument noise, atmospheric, and playa variability is compared to percentage difference between the laboratory calibrated spectra and the Modtran3 constrained independent prediction of radiance.

4.0 Spatial Calibration

The spatial calibration of AVIRIS requires determination of the spatial sampling and spatial response functions and cross-track field-of-view. These data are collected by translating an illuminated narrow slit in the focal plane of a collimator. Measurements are acquired while (1) the AVIRIS scan mirror is in operation and (2) with the scan mirror disabled. The data are analyzed to determine the static and dynamic slit response and the dynamic spatial sampling function (Chrien et al. 1993).

The slit used in the spatial measurements consists of a pair of 100 μm wide gaps separated by 5 mm, etched in a metalized coating on a glass slide. The slit is illuminated by a lamp through a ground-glass diffuser. The entire slit-illuminator assembly is mounted on a computer-controlled translation stage such that the translation is perpendicular to the slit, in the focal plane of the collimator. The effective width of the slit viewed through the collimator is 0.1 milliradians. The slit spacing, width, and translation rate arc measured using a microscope, dial gauges and a stopwatch.

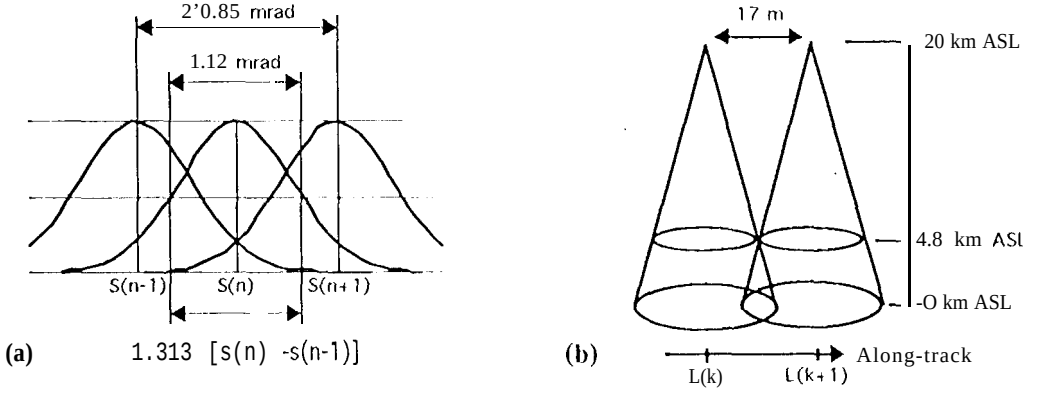

FIGURE 8. Relationship of IFOV and spatial sampling (a) cross-track and (b) along-track

The static IFOV measurements, made in both the cross-track and along-track dimensions, record the slit response versus angular position in milliradians. The FWHM of a best fit Gaussian function is used to describe the static spatial response. The dynamic IFOV is determined in the same way, expect with the AVIRIS whiskbroom scanner in operation. The resultant data set is an image with a set of diagonal stripes. 'l'he peak-normalized detector response for a spatial sample that intersects a stripe versus along-track line is used to derive the dynamic IFOV, the sampling interval in radians, the line-to-line jitter, and the relative alignment between all the spectral channels. The detector readout delay effect (present in pre-1995 data) is no longer present thanks to a new snap-shot mode detector array (which provides simultaneous integration of all spectral channels) which was installed in the AVIRIS sensor prior to the 1995 season.

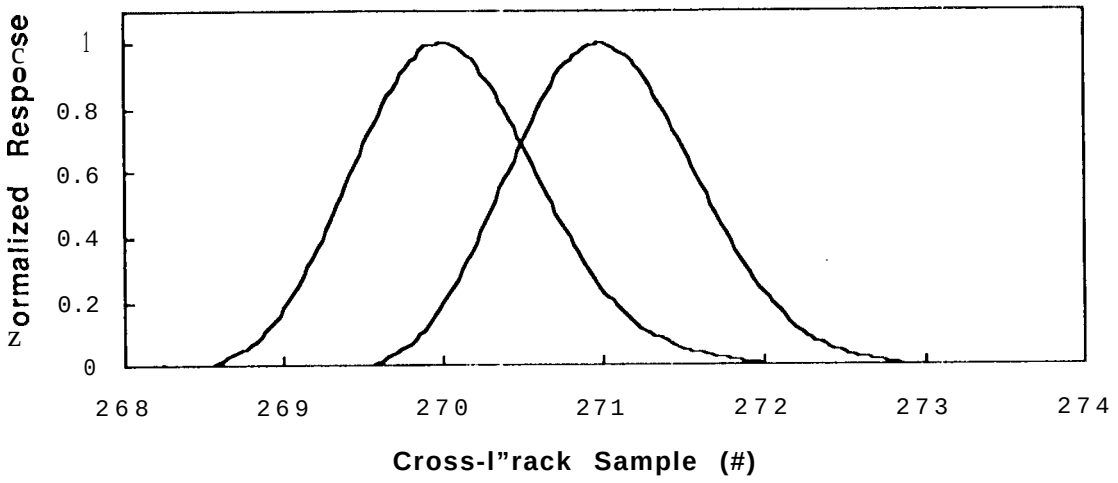

FIGURE 9. Dynamic (scanner-on) cross-track normalized response: Sampling interval is 0.85* FWHM. Asymmetry is the result of residual detector lag present in 1995 AVIRIS data.

Figure 10. shows the normalized spatial response for two consecutive spatial samples of the same detector channel (sample '270 and 271, for channel A030). Units of angular separation can be placed on the x-axis of this plot using the slit translation speed and the 12 Hz line rate and is confirmed by observing the crossing of the second slit. The spacing between adjacent peaks in this curve is the sampling interval and is exactly one spatial sample by definition (0.85 milliradians). The FWHM width of the dynamic spatial response is 1.12 milliradians. The data shown in Figure 10. has been box-car averaged to suppress the effects of line-to-line scan jitter. A comparison of the smoothed and unsmoothed data is used to estimate the line-to-line scan jitter. The data shown in Figure 11. is estimated to have a line-to-line scan jitter 0.08 samples (0.07 milliradians) RMS.

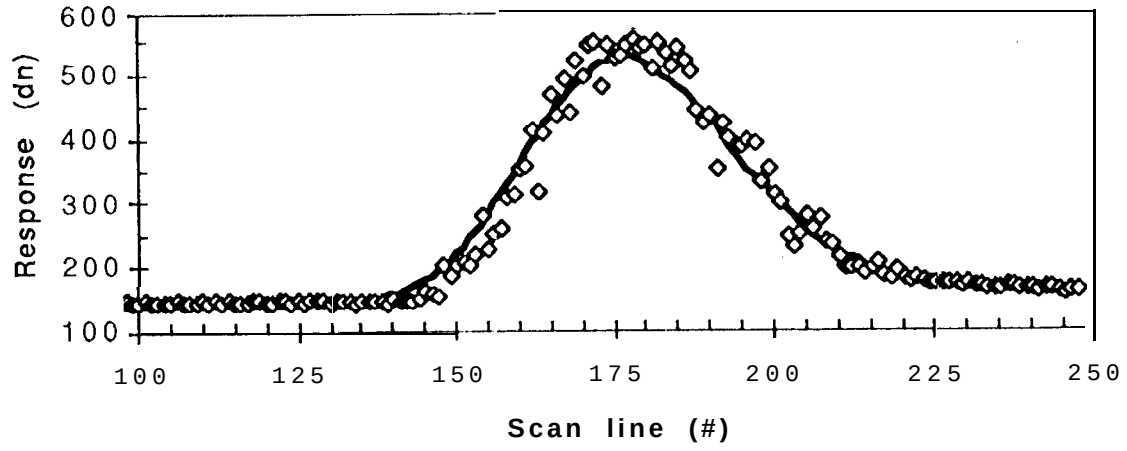

FIGURE 10. Box-car averaged (bold line) and raw (diamonds) dynamic slit response data used to estimate the line-to-line RMS scan jitter.

Ground spot sizes are, as shown in Figure 9. (b), the product of IFOV (in radians) and the aircraft platform altitude above ground level (AGL). While the ratio of cross-track sampling interval to cross-track IFOV remains constant, the along-track sampling interval is a function of the aircraft velocity and the ground height above sea level (ASL) which may vary substantially over mountainous terrain.

The cross-track field-of-view of the AVIRIS sensor is determined by the 614 cross-track samples and the 0.85 milliradians sampling and is 30 degrees in extent. This field-of-view has been confirmed during a scanner over-haul and independently measured by observing the diffraction orders of laser light through a precision Ronchi ruling plate (Chrien, 199 S). Table 1. summarizes the spatial calibration measurements made on 950426 just prior to the 1995 flight season.

TABLE 1. Spatial calibration analysis results from 9S0426 **data set. Variation in IFOV and channel alignment between spectrometers is due to a residual detector lag present in the 1995 AVIRIS data.**

Spectrometer	**A**	**B**	**C**	**D**
Dynamic cross--track IFOV	I. 12 mrad	1.22 mrad	1.16 mrad	1.25 mrad
Line-to--line RMS jitter	0.07 mrad	0.07 mrad	0.07 mrad	0.07 mrad
Cross-track sampling interval	0.85 mrad	0.85 mrad	0.85 mrad	0.85 mrad
Relative channel alignment to A		0.11 mrad	0.09 mrad	0.18 mrad
Static along-track IFOV	1.0 mrad	1.0 mrad	1.0 mrad	1.0 mrad
Static cross-track IFOV	1.0 mad	1.0 mad	1.0 mad	1.0 mrad

5.0 Conclusions

The AVIRIS sensor appears to be meeting the spectral calibration goals of absolute center wavelength knowledge (O. 1nm) and 1 'WHIM bandwidth knowledge (O. 1 nm) across the spectrum. This accuracy holds in-flight as independently validated using solar and atmospheric absorption features. The onboard calibrator spectral filter data (contained in the pre-cal and post-cal files included with every distributed science data set) may be used to sense wavelength calibration changes (due to inadvertent mechanical shock and residual spectrometer instability) with a 0.1 nm sensitivity.

The laboratory determined radiometric calibration coefficients have been shown to valid under actual flight conditions when corrected using the signal from the onboard calibrator. An independently determined radiance based upon the MODTRAN3 code and in situ measurements agrees with the laboratory calibrated AVIRIS data to better then the calibration uncertainty. These results may indicate that NIST over-estimates the radiometric uncertainty of irradiance standard lamps. Laboratory calibrated AVIRIS data appears to be limited by atmospheric correction errors rather than instrumental signal-to-noise ratio, instrument response instability, or laboratory calibration inaccuracies.

Techniques for measuring the AVIRIS spatial characteristics are presented along with a set of results from a recent spatial calibration.

6.0 **Acknowledgments**

'J'his research was carried out by the Jet Propulsion Laboratory, California Institute of Technology, under contract with the National Aeronautics and Space. Administration.

7.0 References

Anderson, G. P., J. Wang, and J. H. Chetwynd, "MODTRAN3: Anupdate and recent validations against airborne high resolution interferometer measurements," Summaries of the Fifth Annual JPL Airborne Earth Sciences Workshop, JPL Publication 95-1, Vol. 1, Jet Propulsion Laboratory, Pasadena, California, pp. 5-8, 1995.

Chrien, 't'. G., M. L. Eastwood, R. O. Green, C. M. Sarture, H. Johnson, C. Chovit, and P. Hajek, "Airborne Visible/Infrared Imaging Spectrometer (AVIRIS) onboard calibration system," Summaries of tbc Fifth Annual JPL Airborne Earth Sciences Workshop, JPL Publication 95-1, Vol. 1, Jet I'repulsion I aboratory, Pasadena, California, pp. 31-32, 1995.

Chrien, T. G., R. O. Green, C. Chovit, M. L. Eastwood, J. Faust, 1'. Hajek, H. Johnson, H. I. Novack, and C. M. Sarture, "New Calibration techniques for tbc Airboroc Visible/tnfrarc.ci Imaging Spectrometer (AVI RI S)" Summaries of the Fifth Annual JPL Airborne Earth Sciences Workshop, JPL Publication 95-1, Vol. 1, Jet Propulsion Laboratory, Pasadena, California, pp. 31-32, 1995.

Chrien, T. G., and R. O. Green, "Instantaneous field of view and spatial sampling of the Airborne Visible/Infrared Imaging Spectrometer (AVIRIS)," Summaries of tbc Fourth Annual JPL Airborne Earth Sciences Workshop, JPL Publication 93-26, Vol. 1, Jet Propulsion Laboratory, Pasadena, California, pp. 23-26, 1993.

Chrien, T. G., R. O. Green, M. L. Eastwood, "Accuracy of the spectral and radiometric laboratory calibration of the Airborne Visible/fnfrared Imaging Spectrometer (AVIRIS)," SPIE Vol. 1298, Imaging Spectroscopy of the Trestle Environment, pp. 37-49, 1990.

Green, R. O., C. Chovit, J. Faust, 1996, "In-flight calibration and validation of the Airborne Visible/Infrared Imaging Spectrometer (AVIRIS) in 1995," Summaries of the Sixth Annual JPL Airborne Earth Sciences Workshop, JPL Publication 96-(in press), Vol. 1, Jet Propulsion laboratory, Pasadena, California, 1996.

Green, R. O., "Determination of the in-flight spectral calibration of AVIRIS using atmospheric absorption features," Summaries of the Fifth Annual JPL Airborne Earth Sciences Workshop, JPL Publication 95-1, Vol. 1, Jet Propulsion Laboratory, Pasadena, California, pp. 71-74, 199S.

Green, R. O., "An Improved spectral calibration requirement for AVIRIS," Summaries of the Fifth Annual JPL Airborne Earth Sciences Workshop, JPL Publication 95-1, Vol. 1, Jet Propulsion I aboratory, Pasadena, California, pp. 75-78, 1995.

Green, R. O., J. E. Conel, M. Helmlinger, J. van den Bosch, C. Chovit, and T. G. Chrien, "Inflight calibration of AVIRIS in 1992 and 1993," Summaries of tbc Fourth Annual JPL Airborne Earth Sciences Workshop, JPL Publication 93-26, Vol. 1, Jet Propulsion Laboratory, Pasadena, California, pp. 69-72, 1993.

Green, Robert O., "Usc of Data from the AVIRIS Onboard Calibrator," Summaries of the Fourth Annual JPL Airborne Earth Sciences Workshop, JPL Public 93-26, 1993.

Green, Robert O., Steve Larson anti Ian Novack, "Calibration of AVIRIS digitized data", Proc. Third Annual Airborne Geoscience Workshop, JPL Publication 92-14, pp. 1992

Sarture, C. M., T. G. Chrien, R. O. Green, M. L. Eastwood, J. J. Rant.y, and M. A. Hernandez, "Airborne Visible/Infrarcci imaging Spectrometer (AVIRIS) sensor improvements for 1994 and 1995," Summaries of the Fifth Annual JPL Airborne Earth Sciences Workshop, JPL Publication 95-t, Vol. 1, Jet Propulsion Laboratory, Pasadena, California, pp. 145-148, 1995.

Vane, G., R. (J. Green, T. G. Chrien, }1. 1'. Enmark, E. G. Hansen, and W. M. Porter, "The Airborne Visible/Infrarcd imaging Spectrometer (AVIRIS)," Remote Sens. Environ., 44:127-143 (1993).

Vane, G. 'T. G. Chrien, E. A. Miller, J. H. Reimer, "Spectral and radiometric calibration of the Airborne Visible/Infrared imaging Spectrometer," SPIE Vol. 834, Imaging Spectroscopy II, pp. 91-105, 1987.